

Validation and Analysis of the Propagation Channel at 60 GHz for Vehicular Communication

Maximilian Lübke¹, Jonas Fuchs¹, Anand Dubey¹, Hussein Hamoud¹, Falko Dressler², Robert Weigel¹
and Fabian Lurz³

¹Institute for Electronics Engineering,
Friedrich-Alexander-Universität Erlangen-Nürnberg, Cauerstr. 9, 91058 Erlangen, Germany

²School of Electrical Engineering and Computer Science,
Technische Universität Berlin, Einsteinufer 25, 10587 Berlin, Germany

³Institute of High-Frequency Technology,
Hamburg University of Technology, Denickestr. 22, 21073 Hamburg, Germany

E-mail: {maximilian.luebke, jonas.fuchs, anand.dubey, hussein.hamoud, robert.weigel}@fau.de,
dressler@ccs-lab.org, fabian.lurz@tuhh.de

Abstract—The use of millimeter wave communication gets more and more attention with the growth of 5G, particularly with regard to promising applications like platooning or intersection assistant. However, for the design of those applications, a clear understanding of the channel behaviour at these frequencies is mandatory. Aiming to fill the gap of missing channel models for frequencies above 60 GHz, this paper investigates the channel characteristics necessary for future vehicular applications. Based on the commercially available channel simulation tool WinProp, Altair, a typical vehicular scenario in the city center of Berlin (Germany) is analysed. The simulation results are verified with channel sounding measurements at 60 GHz. Hereby, the dependency of the channel with respect to scatterers like trucks and cars is evaluated. Reflection paths were found to be up to 30 dB higher in received power compared to scattering ones. Further, a platooning scene, consisting of 20 vehicles driving towards each other while communicating, is investigated for various time steps and receiver points. In this context, different antenna types are introduced to reduce interfering signals nearby the major transmitter, achieving a decrease in interference power of up to 20 dB.

Index Terms— channel simulation, ITS, platooning, 60 GHz.

I. INTRODUCTION

In the context of vehicle-to-vehicle (V2V) communication, millimeter waves (mmWaves) are gradually in the spotlight, especially with the rise of 5G. Besides the already implemented standards like IEEE 802.11p and LTE, approaches investigating the usage of higher frequencies with the benefits of higher antenna gains and usable bandwidth are known in the literature [1]. With the upcoming utilization of 5G, frequencies above 60 GHz (e. g. the 76-81 GHz band for automotive applications) or even frequencies above 100 GHz are investigated [2].

Utilizing those frequencies is particularly advantageous as they are already used in sensor technologies of modern vehicles. However, intelligent transportation systems (ITS) of today call additionally for communication approaches to support efficient and safety aware applications like platooning or an intersection assistant. Therefore, RADar based COMMunication (RADCOM) can offer a new alternative to the existing standards

by being capable of sensing and communicating at the same time utilizing the same signal. Thus, the set of current standards is completed by RADCOM.

Although measurement campaigns exist in the context of 5G, there is still a lack of propagation models in this frequency range [3]. Consequently, channel characteristics are not fully explored yet [4], [5]. To address this issue, few channel simulators are available. Besides stochastic simulators like NYUSIM [6], commercial solutions like Wireless Insite¹ or the deterministic simulation tool WinProp² are in use. In previous work, WinProp and NYUSIM, were compared regarding their individual (dis-) advantages, showing that WinProp simulation to be highly accurate to real measurements [7]. The simulation results allow first impressions in understanding the anticipated propagation, as proposed by B. Colo et al. in [8]. However, fully valid channel models are still not part of state-of-the-art simulation frameworks like Veins [9] or Artery [10].

In the proposed paper, our ongoing research and the achieved results regarding the characterization of the channel at 60 GHz using the simulation tool WinProp are presented. Our key contributions are:

- we verify and validate the simulation results against measurements regarding the power delay profiles (PDPs);
- we investigate the propagation effects of a typical street scenario in Berlin, Germany;
- we further evaluate the impact of additional scatters; and
- we evaluate platooning in this urban scene, applying different antenna characteristics and investigating a dynamic scene.

II. MMWAVE CHANNEL

To satisfy the demand for higher data rates and capacity in the automotive sector, the switch to higher frequencies in the mmWave range is mandatory. Therefore, the knowledge about

¹www.remcom.com/wireless-insite-em-propagation-software

²www.altairhyperworks.com/WinProp

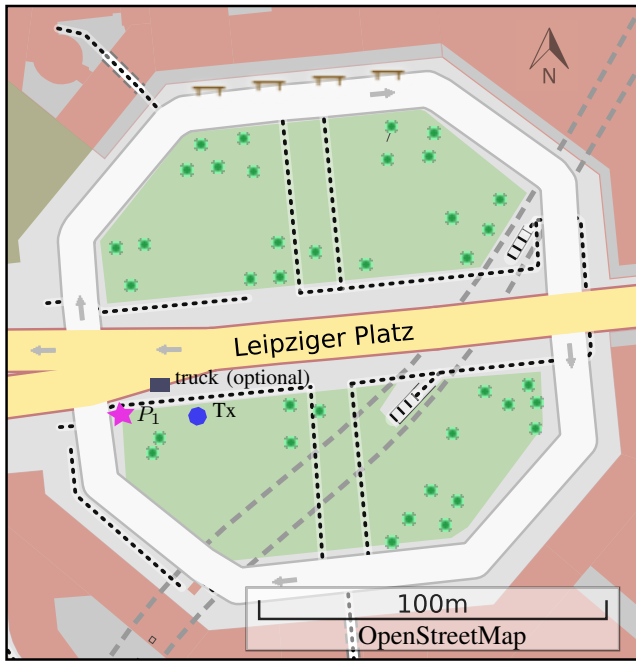


Fig. 1. Map of "Leipziger Platz" in the city center of Berlin. The blue octahedron corresponds to the transmitter position, the violet star to the receiver position and the truck in form of the grey square is evaluated for the later observations.

the channel in that frequency range is absolutely necessary as propagation effects like reflection or scattering influence the communication signals significantly. Especially, in the event of safety relevant information, the fluctuation can lead to missed messages and in consequence to critical situations.

To evolve channel models, measuring is the most reliable but also the most cost and time intense method. However, the available measurement campaigns are rather limited, especially in the context of mmWave communication, due to the great diversity of traffic scenarios. Nevertheless, several typical scenes for indoor and outdoor applications were gauged by [6], [11], [12].

Another approach, reducing the time and cost disadvantages, is to apply stochastic or deterministic simulation tools. In this paper, the focus lies on a realisation via the deterministic simulation tool WinProp, Altair. The channel is described with respect to the impact of obstacles or dynamic channel behaviour. Within WinProp, scenarios can be built up with a high level of detail but the results are highly linked to this scene. However, WinProp is capable of determining the electromagnetic wave propagation for a large variety of automotive scenarios, whether it be urban, rural or mixed forms. Therefore, WinProp is well-established in research to study the channel propagation [8], [13], [14]. In the following, the configuration and the validation of WinProp is explained, after the considered simulation environment is introduced.

A. Simulation Environment – Leipziger Platz

The proposed scene is adapted from the "Leipziger Platz", located at the city center of Berlin (Germany). The scenario

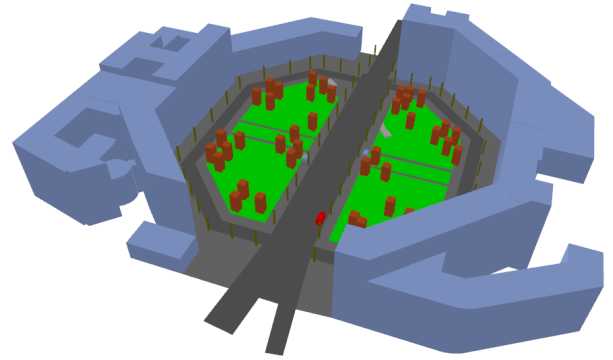


Fig. 2. 3D-model of the "Leipziger Platz" reconstructed in WinProp (v.2019.3.3). The contained materials are coloured separately according to their characteristics.

based on OpenStreetMap is depicted in Fig. 1. It is shaped similar to an open square of octagonal shape with a diameter of approximately 150 m and is flanked by glass and stone buildings. The high street widens up from 4 lanes outside the square to 6 lanes inside the square. Additionally, streets with two driving lanes and wide sidewalks lead around the place, whereas grass strips with trees can be found inside. The receiver is set to a height of 1.5 m at the position P_1 , highlighted as violet star, and the transmitter at height of 3.5 m, marked as a blue octahedron. By doing so, the scenario models a street lamp, representing a typical roadside unit (RSU), communicating via vehicle-to-everything (V2X) with pedestrians, cyclists or vehicles. Additional scatterers, like the truck (grey square), will influence the channel characteristics significantly. This impact will be evaluated in section III-B.

Based on open street maps, the individual streets, green strips, sidewalks, lampposts, bus stops, trees and other details were reconstructed and modeled accordingly in WallMan. The corresponding model is shown in Fig. 2. The various colours represent different material properties, as they can be defined in WallMan for each object individually and even frequency dependent.

B. WinProp Configuration

In WinProp various models, such as empirical, semi-empirical and ray-optical ones, are included. However, in the proposed paper, the ray-tracing approach was applied. The simulation is based on Fresnel equations, the geometrical theory of diffraction and the uniform theory of diffraction to observe the reflection, transmission and diffraction loss. Within the simulation, material parameters, like permeability μ_r , permittivity ϵ_r and conductivity σ have to be set. Therefore, the buildings are assumed as glass, the trees as wood, the streets as concrete and the sidewalks as concrete plaster. The street lamps were chosen to be highly conductive. According to the literature recommendation, the material characterization were defined as follows: glass is assumed to have an $\epsilon_r = 8.9 - j0.13$, trees $\epsilon_r = 1.57 - j0.096$ and concrete $\epsilon_r = 6.14 - j0.3$ at 60 GHz. The permeability μ_r is equal to 1 for all materials [15].

Furthermore, the propagation parameters had to be chosen. The transmit power was set to 15 dBm at a center frequency of 60 GHz with a quasi omnidirectional antenna pattern. This is according to the measurement campaign, which will be used for validation of the deterministic simulation [16]. Thus, an antenna gain of 2 dBi was set.

In the simulation up to three reflections and one transmission besides scattering were evaluated. The spatial resolution δ of the scene was defined to 0.6 m according to

$$\delta = \frac{c}{2 \cdot B}, \quad (1)$$

with respect to the measurement bandwidth B of 250 MHz and the constant c corresponding to the speed of light in vacuum. Limiting the dynamic of the receiving power to 200 dB, the 500 strongest paths in reception strength were computed and analysed individually, regarding path loss, delay, direction of departure, direction of arrival, Doppler shift and the underlying propagation effects. The simulation parameters against the measurement parameters are summarized in Table I.

TABLE I
SUMMARY OF THE CHOSEN MEASUREMENT AND SIMULATION
PARAMETERS USED FOR VALIDATION.

	WinProp	Measured [16]
Carrier Frequency	60 GHz	60 GHz
Bandwidth B	250 MHz (Eq. 1)	250 MHz
Transmit Power	15 dBm	15 dBm
Antenna Gain	2 dBi	2 dBi
Observation Time	static	averaged 50 s
Tx Antenna Height	3.5 m	3.5 m
Rx Antenna Height	1.5 m	1.5 m

C. Validation

The results of the model, available at [17], were compared with the measurement campaign from [15], [16], [18] in order to evaluate the reliability and consistency of simulation and measurement. The first mandatory effort was to reconstruct the environment of the "Leipziger Platz" in a very detailed way, resulting in the 3D-WallMan-model shown in Fig. 2. The measured data and the simulated propagation paths are depicted in Fig. 3.

Fig. 3 reveals that there are several strong paths measured, highlighted in the solid blue line, at 276 ns, 308 ns and 324 ns additional to the line-of-sight (LOS) path at 82.6 ns delay. The LOS component corresponds to a Tx-Rx distance of 24.8 m with an observed averaged path loss of approximately 96 dB for a 50 s measurement [18]. The simulation results are shown in dashed red diamonds at an equivalent position to the predefined position P_1 . The LOS path with 82.7 ns and path loss 96 dB is consistent with the measurement. The other peaks are also in the same amplitude and delay range, whereas detecting the exact values of the measured paths is unrealistic, e. g. due to simplifications in the geometry. Additional to a peak at 249 ns delay with a corresponding 124.5 dB path loss, peaks at 297 ns (113.3 dB), 164 ns (124.5 dB) and 205 ns (127 dB) are predicted. This matches with the measured shape. Moreover, R. J. Weiler

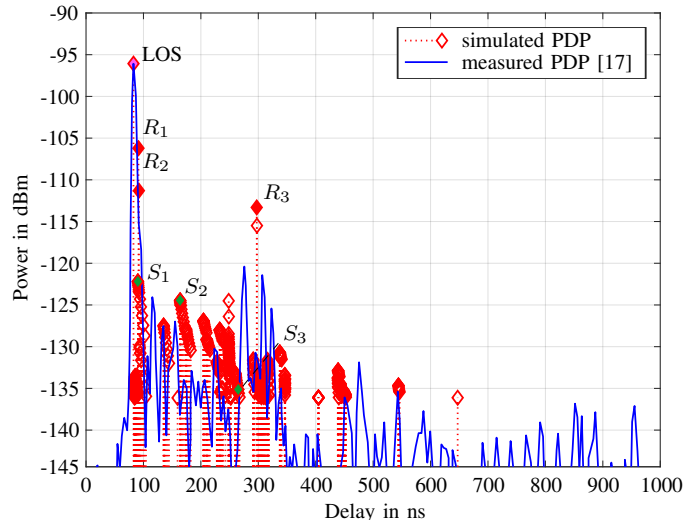


Fig. 3. Simulated and measured (according to [16]) power delay profile (PDP) analysed at position P_1 . The corresponding reflection (R_i) and scattering (S_i) paths in filled red and green diamonds and their origin are depicted in Fig. 4.

et al. (2016) observed a 1-2 dB power fluctuation of the stable components in their proposed results [16].

By comparing the simulation results to the measurements, the peaks are significantly wider in the measured setup due to the maximum bandwidth B of the channel sounder of 250 MHz. Although, within this setup of the simulation the carrier frequency and the resolution δ of the prediction results were defined to 0.6 m accordingly, the observed peaks are really narrow in terms of temporal resolution. This explains the difference in the first peaks around 100 ns. The peaks at 91 ns (106 dB) and 92 ns (111 dB) are included in the wide peak at 100 ns in the measurement results. The slight difference in delay can be explained by receiver and transmitter placement as it is inherently inaccurate. Simultaneous variations in the antenna placement – with a constant Tx-Rx distance of 24.8 m – led to slight differences in the peak delays. The LOS path does not differ in delay and path loss from the original setup, as the direct connection remains without obstacles in between. However, most of the paths will change as the distances between the objects in the environment varies and, therefore, waves are received with different delays and path losses. Considering the higher delays, the simulation shows a cut at 647 ns, whereas in the measurements delays over 900 ns can be observed. This is due to the predefined limitation to 500 considered paths, resulting in a disregard of paths with a delay higher than 647 ns.

III. RESULTS

Since approximations are unavoidable in simulations and thus cannot comprehensively represent the reality, the propagation paths are further analysed and compared to the measurement results. This provides the basis for further channel characterizations with respect to its dynamic behaviour like by including additional obstacles.

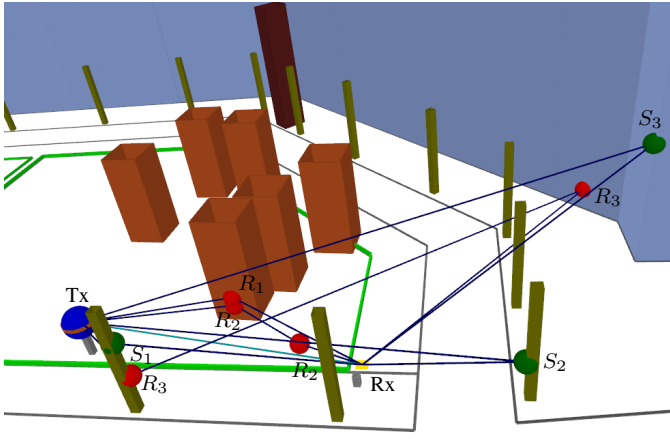


Fig. 4. Selected propagation paths simulated in WinProp. The colour of the dots represents the different propagation effects. Green ones correspond to scattering, whereas red dots correspond to a reflection. The blue dot displays the Tx position and the yellow area the receiver. The LOS path is coloured in turquoise.

A. Propagation Paths

The origin of the received multipaths will be addressed in the following. R. J. Weiler et al. assumed that besides the LOS path, mainly the surrounding buildings act as reflectors and, therefore, caused the observed multipaths [16]. In WinProp, the individual paths including the occurring propagation effects—transmission, reflection, diffraction, scattering—can be resolved. In Fig. 4, a selection of different propagation paths is depicted in a 3D-view. Thus, the assumption can be confirmed as the paths, marked in red in Fig. 3, have their origin in a reflection at the buildings (red dots in Fig. 4). Moreover, also paths with multiple reflections, like R_2 or R_3 , appear. Scattering at the trees and the ground is highlighted as green diamonds in Fig. 3 and as green dots in Fig. 4, respectively. However, the highest peaks besides the LOS path are caused by reflection, marked as red point, at the street lamp, trees and the ground. Scattered waves are significantly lower in amplitude than reflections from buildings (compare S_3 - R_3). In general, it is obvious that the observed paths are highly dependent on the considered scene.

This provides an explanation of the slight differences between the detected components in the simulation results compared to the measurement. The modelled environment will not match the real measurement scene exactly. Missing peaks in the simulation results, like the one at 276 ns, could be caused by a missing strong reflector of the measurement environment in the modelling. This problem can hardly be solved since it would require to reconstruct the whole surroundings and material parameters exactly for occasionally fast changing scenes. However, this is unrealistic, time and cost expensive and in this case not necessary as the differences are relatively small. Nevertheless, it is crucial to look at the dynamic channel behaviour that has to be expected in real traffic to get a deeper understanding of the channel. This information in turn is needed

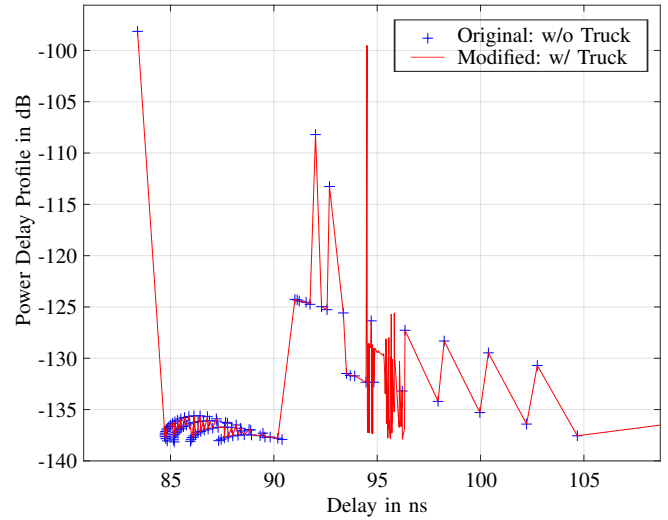


Fig. 5. Simulated power delay profile analysed at position P_1 with (w/) and without (w/o) an additional truck included in the simulation environment. The position of the truck is displayed as grey square located in Fig. 1.

to design the communication in a proper way. Especially for ITS safety relevant applications, such as intersection assistant, this is even more important. Therefore, in the next section the scenario was changed and the consequential effects were investigated.

B. Obstacles

To show the dynamic effects of the channel at 60 GHz, vehicles are considered in the simulation. Exemplary, a truck with 5265 mesh elements and a height of 3.5 m was included on the street between the transmitter and the receiver (compare Fig. 1). The material of the vehicles was set to be highly conductive with $\sigma = 27778 \text{ S}\cdot\text{m}^{-1}$, $\epsilon_r = 1$ and $\mu_r = 20$. Transmissions inside the truck were excluded. The simulation results with and without the truck are shown in Fig. 5. For clarity reasons, only the part which differs most from the previous simulation results is displayed. The profile above 100 ns has only negligible differences to the previous simulation, as the environment, trees, buildings etc., apart from the added truck, remains unchanged. Until a delay of 94.5 ns, there is also no observable change. The power delay profile of the original simulation, marked with blue crosses, is identical with the modified one, displayed as a solid red line. However, some propagation paths with low amplitude, especially for the higher delays, are not displayed, as they do not belong to the 500 strongest paths anymore. Like in Fig. 4, the red dots correspond to reflections and the green ones to scattering. In comparison to Fig. 4 the truck acts particularly as a scatterer and a reflector. The scattering and reflection paths from the environment itself remain the same.

Compared to the simulation without the truck (blue cross in Fig. 5), new propagation paths appeared in a range of 94.5 ns to 96.2 ns delay for the modified simulation (red solid line). Close to 50+ additional scattering paths, which all have a path loss off around 130 dB and one outstanding reflection path with

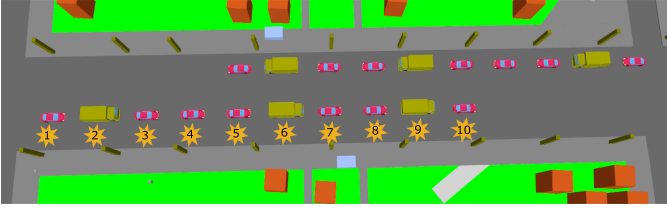


Fig. 6. Considered platooning scenario. 20 vehicles are organized in two separate platoons, all driving with a speed of 10 ms^{-1} towards each other. The vehicles of the lower platoon act as transmitters (numbered from 1–10), whereas the vehicles of the upper platoon represent the receivers.

a path loss of 99.5 dB can be observed. The transmitted wave is reflected at the truck and propagates directly to the receiver, leading to this peak. In consequence, this 30 dB difference between a few nanoseconds, indicates how dynamically the received power can change. Thus, this additional peak can have a significant impact on the communication link and gets even more severe in non-line-of-sight (NLOS) communications, where the strong LOS peak will not be received. These changes of scattering and reflection paths will cause high fluctuations in receiving power, which needs to be resolved for future applications for ITS.

C. Platooning

To extend the scenario to a more vehicular communication related one, a typical platooning scene is evaluated in the next step. Therefore, two platoons were added to the original scene. In Fig. 6, the considered platoons, containing 10 vehicles, either trucks or cars each, all driving with the same speed level of 10 ms^{-1} , are shown. The materials of the cars and trucks are chosen to be the same as the truck in the previous section. Also there were only minor changes of the simulation configurations with respect to the aforementioned parameter set. Up to four reflections, scattering and one transmission were calculated. Eight time steps, at an interval of 1 s, were evaluated.

All vehicles of the lower lane/platoon are acting as transmitters, whereas the vehicles of the upper platoon receive the signals. At first, the received signals at the platoon leader in the upper lane are investigated exemplarily. All ten vehicles of the lower platoon are transmitting simultaneously to search for the best transmitter position while evaluating the communication link of different transmitter-receiver pairs and the worst case interference between them. As safety relevant information about upcoming traffic or for intersection management should be exchanged, mutual interference has to be minimized. Both the transmitter and the receiver antennas are mounted at the front bumper of the individual vehicle at a height of 0.5 m. A power of 15 dBm is emitted at 60 GHz and the received signals are simulated (a) for omnidirectional antennas (b) for an 60 GHz focussed antenna with 12.38 dBi antenna gain. The antenna directivity is shown in Fig. 7. It has a half power beamwidth of 36.25° in azimuth, whereas the side lobe level is -11.99 dB . As the efficiency is set to 1, the directivity and the gain are equal. The antennas are oriented straight forward towards the vehicles in their platoon. The received signals are evaluated

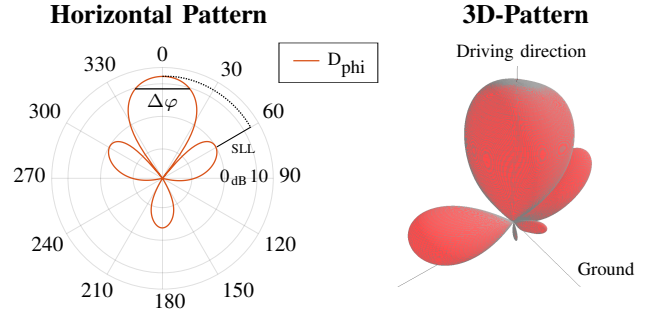


Fig. 7. Both horizontal and 3D-pattern of the considered 60 GHz antenna. The directivity of the antenna is depicted. It has a sidelobe level (SLL) of -11.99 dB and a half power beamwidth in azimuth of $\Delta\varphi = 36.25^\circ$.

for the different antenna characteristics as well as for varying time steps to extend the interference analysis of Petrov et al. (2018) [19].

Furthermore, the power delay profiles and the observed root mean square (rms) delay spread τ_{rms} are estimated according to the following equations

$$\bar{\tau} = \frac{\int_0^\infty \tau P_h d\tau}{\int_0^\infty P_h d\tau}, \quad \tau_{\text{rms}} = \sqrt{\frac{\int_0^\infty (\tau - \bar{\tau})^2 P_h(\tau) d\tau}{\int_0^\infty P_h(\tau) d\tau}}, \quad (2)$$

where τ represents the delay, $\bar{\tau}$ the mean delay of the channel and P_h the received power, respectively. The whole set of results, including PDPs and τ_{rms} for all eight time steps as well as the ten transmitters and ten receivers, are public available at [20].

Omnidirectional antenna characteristics: For the omnidirectional case, the power delay profile of the first time step is depicted in Fig. 8a, corresponding to the scene shown in Fig. 6. The PDPs of the transmitter signals clearly overlap, causing interference which is especially distorting the dominant received signal. As the scene, depicted in Fig. 6, is analysed, the dominant signals are transmitted from the vehicle positioned at '4' ($P_{\text{max}} = -74 \text{ dBm}$; $\tau = 36 \text{ ns}$) and with minor attenuation from vehicle '3' ($P_{\text{max}} = -78 \text{ dBm}$; $\tau = 58 \text{ ns}$) and from the truck at '2' ($P_{\text{max}} = -81 \text{ dBm}$; $\tau = 82 \text{ ns}$). These are all either LOS or (ground-) reflections paths. The three transmission unites also the resulting low τ_{rms} of roughly between 10 and 19.2 ns.

The received signals also for the remaining transmitters show three clusters, having various propagation paths and effects, respectively: Paths up to 260 ns delay include the highest receiving powers as they have their origin in the LOS path and reflections at the vehicles, the ground or/and the environment (trees, street lamps, ground edges). Additionally, this first cluster contains scattering at the nearby environment, like street lamps and trees, with signal receiving powers in the range of -110 to -130 dBm . In the second cluster, ranging from approx. 320 ns to 460 ns delay (depending on which transmitter is active), mainly scattering at trees and few primal scatterings at buildings can be observed. Some peak values, e. g. at transmitter position '1', '2' or '3', of approx. -112 dBm have their origin in reflections at trees and thus, stand out the

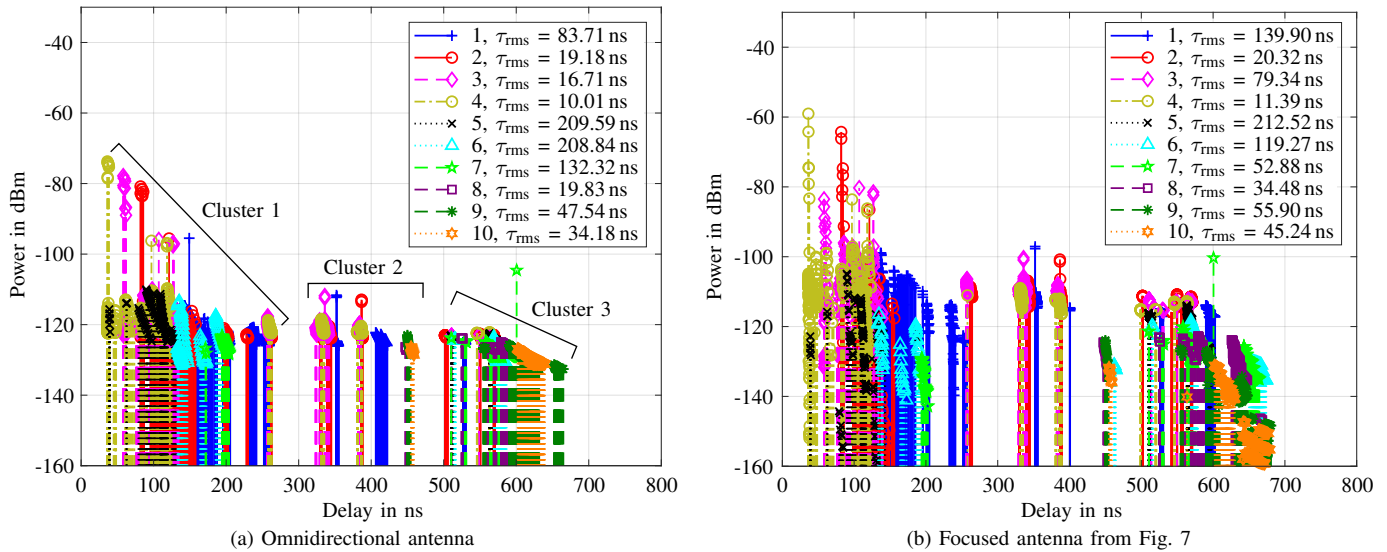


Fig. 8. Power delay profiles and the corresponding τ_{rms} received at the upper platoon leader at time step $t = 0$ s. The different colors represent the different transmitter positions. The numbering is according to Fig. 6. Three time clusters can be observed.

receiving powers of the surrounding scattering paths of roughly -120 dBm to -130 dBm. Scattering at buildings are, however, mostly existent in the third cluster from 500 ns to 665 ns delay and receiving powers smaller than -120 dBm. Nevertheless, reflections in this cluster can peak, like the received signals of transmitter '7' with a power of -104 dBm. It is caused by two reflections from the truck in position '6' and buildings, respectively. However, the vehicles, which are in position '5-10', only have a minor influence on the communication, as there is only a NLOS communication possible. Most of the signals are scattered by mid-range environment or the far-off buildings, but do not have a significant influence, if there is a LOS path available. Nevertheless, especially for pure NLOS cases, those signals can play an important role to receive any signals or support the communication link in receiver structures for example in rake receiver designs. Of course, the observed rms delay spread τ_{rms} for the transmitter '5-10' is higher than for the LOS cases. This is particularly for transmitter positions '5' and '6' true where even if there is only NLOS paths available, many signals are still received, whereas for '8-10' only signals out of the last cluster are observed.

Antenna characteristics (see Fig. 7): Subsequently, the idea to reduce distortion and interference by applying beam formed antennas both for the transmitters and the receiver, is evaluated exemplary for an antenna characteristic, presented in Fig. 7. Again, the power delay profiles for the entire set of transmitting vehicles located at the lower platoon and the platoon leader acting as receiver are depicted in Fig. 8b at time step $t = 0$ s. One can see the cars driving through the street with different obstacles like vegetations, buildings around and thus, observing completely different PDPs over time. Thereby, three dominant time clusters can be spotted, same as for the omnidirectional case. For the omnidirectional antenna, however, the received signals result in a high amount of interference, especially for the most important received signal (from vehicle positioned at

'4' with $P_{max} = -74$ dBm; $\tau = 36$ ns). This should be solved by using a focused antenna.

The corresponding PDPs are highlighted in brown dashed circles (transmitter positioned at vehicle/car '3'), solid red circles (at vehicle/truck '2') and dotted black crosses (at vehicle/car '5') in Fig. 8b. While the dominant path experiences an amplification from -74 dBm to now -59 dBm, speaking about a gain of 15 dB, the signals of the transmitters '3' and '5', located nearby the dominant '4' transmitter, are getting reduced or at least not amplified. The receiving power, transmitted by '3', decreases from -78 dBm for omnidirectional antennas to -83 dBm for the focused antennas. The same applies to the receiving power out of '5' which is also close to the dominant path of '4'. Its originally -81 dBm receiving power reduces to even -123 dBm. In consequence, the receiving power and therefore, the most prominent communication link between the '4' vehicle and the receiving leader of the upper platoon is getting significantly less disturbed. This is also indicated by the increase of τ_{rms} of '3' from 16.71 ns to 79.34 ns and the constant high one of '5' at over 200 ns for an applied antenna, whereas τ_{rms} of '4' still remains roughly constant at 11.39 ns.

Moreover, the reduction in receiving power see in the third cluster as well. Scattering at far environment (trees, street lamps, buildings) can be received of course only with a clear drop in amplitude. Additionally, by utilizing the focused antenna 'omnidirectional' propagation paths are replaced by other scattering paths. In general, those paths have a notable reduced receiving power, too. Here the evaluation of only the 500 most dominant paths is a limiting factor. The rest of the paths in cluster three, like the reflection peak of '7', are only slightly amplified by 4 dB.

Compared to cluster '3', the signals (reflections, scattering at the midrange environment) of cluster '2' are amplified considerably more about roughly 10 dB. This increase is also observable for the signals coming from the nearby environment

of cluster '1'. Particularly, reflection paths with transmitters at '2'-'4' getting amplified by up to 16 dB. However, the most dominant paths are still the LOS and ground reflection paths of '4' and '2', whereby '3' is reduced as aforementioned.

Additional observations: The trend of reducing the nearby signals of the major transmitter signals as well as decreasing in receiving power of scattering signals of the latest cluster in general, behaves similarly for later time steps and for other prediction points. However, for larger distances between the transmitters and the receiver for both the omnidirectional antennas but also for the focused antennas, this is even enhanced, resulting in up to no longer available communication links. At this point, the authors want to reference the open access data set [20] once again, where the entire set of simulation results for all the other prediction points and time steps are public available.

IV. CONCLUSION

In this paper, a data basis for future research regarding detailed channel models for mmWaves at 60 GHz is proposed to overcome the lack of channel models for these frequencies. Utilizing the deterministic channel simulator WinProp, a typical platooning scene in the city center of Berlin (Germany) was reconstructed, evaluated and validated with real measurements. The results of the 3D-ray-tracing (online available at [17]) showed good agreement with the measurements and therefore, validate the use of WinProp for mmWave channel analysis even for frequencies above 60 GHz. Particularly reflection paths resulted in the highest receive power, while some paths are missing in the simulation results as there is a great dependency on the considered environment, especially on the obstacles. Thus, changes of up to 30 dB in path loss can be observed if reflection paths become possible.

To address V2V related applications, a platoon, with 20 vehicles (cars, trucks) driving towards and simultaneously communicating with each other, was evaluated for eight time steps as well as for ten prediction points. Besides the deep analysis of the propagation delay and the root mean square delay spread, the propagation paths and their underlying propagation effects were investigated. The observed strong interference of the dominant path for omnidirectional transmitter and receiver antennas was solved by introducing focused antennas, reducing the nearby signals of minor relevant transmitters to 20 dB difference in power within 23 ns difference.

Evaluating the channel and finding a suitable channel model for 60 GHz but also for automotive frequencies around 77 GHz at various environments (urban, rural, high ways) is the main goal of our future research. The gained channel models will be integrated into more realistic vehicular communication models to analyse and optimise future ITS applications.

ACKNOWLEDGMENT

The authors wish to acknowledge the assistance and support of the Deutsche Forschungsgemeinschaft, DFG within the project 390837865 and their project partner, the CCS Labs.

REFERENCES

- [1] C. Sommer and F. Dressler, *Vehicular Networking*. Cambridge University Press, 2014.
- [2] I. A. Hemadeh, K. Satyanarayana, M. El-Hajjar, and L. Hanzo, "Millimeter-wave communications: Physical channel models, design considerations, antenna constructions, and link-budget," *IEEE Communications Surveys & Tutorials*, vol. 20, no. 2, pp. 870–913, 2017.
- [3] R. He, B. Ai, G. Wang, Z. Zhong, C. Schneider, D. A. Dupleich, R. S. Thomae, M. Boban, J. Luo, and Y. Zhang, "Propagation Channels of 5G Millimeter-Wave Vehicle-to-Vehicle Communications: Recent Advances and Future Challenges," *IEEE Vehicular Technology Magazine (VTMag)*, vol. 15, no. 1, pp. 16–26, Mar. 2020.
- [4] E. Ben-Dor, T. S. Rappaport, Y. Qiao, and S. J. Lauffenburger, "Millimeter-Wave 60 GHz Outdoor and Vehicle AOA Propagation Measurements Using a Broadband Channel Sounder," in *IEEE GLOBECOM 2011*, Houston, TX: IEEE, Dec. 2011, pp. 1–6.
- [5] S. Sun, G. R. MacCartney, and T. S. Rappaport, "A novel millimeter-wave channel simulator and applications for 5G wireless communications," in *IEEE ICC 2017*, Paris, France: IEEE, May 2017.
- [6] M. K. Samimi and T. S. Rappaport, "3-D millimeter-wave statistical channel model for 5G wireless system design," *IEEE Transactions on Microwave Theory and Techniques*, vol. 64, no. 7, pp. 2207–2225, 2016.
- [7] M. Lübke, S. Dimce, M. Schettler, F. Lurz, R. Weigel, and F. Dressler, "Comparing mmWave Channel Simulators in Vehicular Environments," in *2021 IEEE 93rd Vehicular Technology Conference (VTC2021-Spring)*, 2021, pp. 1–6.
- [8] B. Colo, A. Fouda, and A. S. Ibrahim, "Ray Tracing Simulations in Millimeter-Wave Vehicular Communications," in *IEEE PIMRC 2019*, Istanbul, Turkey: IEEE, Sep. 2019.
- [9] C. Sommer, R. German, and F. Dressler, "Bidirectionally Coupled Network and Road Traffic Simulation for Improved IVC Analysis," *IEEE Transactions on Mobile Computing (TMC)*, vol. 10, no. 1, pp. 3–15, Jan. 2011.
- [10] R. Riebl, H.-J. Günther, C. Facchi, and L. Wolf, "Artery - Extending Veins for VANET Applications," in *MT-ITS 2015*, Budapest, Hungary: IEEE, Jun. 2015.
- [11] T. S. Rappaport, E. Ben-Dor, J. N. Murdock, and Y. Qiao, "38 GHz and 60 GHz angle-dependent propagation for cellular & peer-to-peer wireless communications," in *IEEE ICC 2012*, Ottawa, Canada: IEEE, Jun. 2012.
- [12] G. R. MacCartney and T. S. Rappaport, "73 GHz millimeter wave propagation measurements for outdoor urban mobile and backhaul communications in New York City," in *IEEE ICC 2014*, Sydney, Australia: IEEE, Jun. 2014.
- [13] R. Hoppe, G. Wolffe, P. Futter, and J. Soler, "Wave propagation models for 5g radio coverage and channel analysis," in *APCAP 2017*, Xi'an, China: IEEE, Oct. 2017.
- [14] Z. Zhang, J. Ryu, S. Subramanian, and A. Sampath, "Coverage and channel characteristics of millimeter wave band using ray tracing," in *IEEE ICC 2015*, London, United Kingdom: IEEE, Jun. 2015.
- [15] M. Peter, R. Weiler, B. Göktepe, W. Keusgen, and K. Sakaguchi, "Channel measurement and modeling for 5G urban microcellular scenarios," *MDPI Sensors*, vol. 16, no. 8, p. 1330, 2016.
- [16] R. Weiler, M. Peter, W. Keusgen, A. Maltsev, I. Karls, A. Pudseyev, I. Bolotin, I. Siaud, and A.-M. Ulmer-Moll, "Quasi-deterministic millimeter-wave channel models in MiWEBA," *EURASIP Journal on Wireless Communications and Networking*, vol. 2016, Dec. 2016.
- [17] M. Lübke and S. Dimce, *Validation Data for WinProp and NYUSIM*, version 1.0.0, Zenodo, Sep. 2020. [Online]. Available: <https://doi.org/10.5281/zenodo.4047979>.
- [18] R. Weiler, M. Peter, W. Keusgen, and M. Wisotzki, "Measuring the busy urban 60 GHz outdoor access radio channel," in *IEEE International Conference on Ultra-WideBand (ICUWB 2014)*, Paris, Sep. 2014.
- [19] V. Petrov, J. Kokkonen, D. Moltchanov, J. Lehtomäki, M. Juntti, and Y. Koucheryav, "The Impact of Interference From the Side Lanes on mmWave/THz Band V2V Communication Systems With Directional Antennas," *IEEE Transactions on Vehicular Technology*, vol. 67, no. 6, pp. 5028–5041, 2018.
- [20] M. Lübke and H. Hamoud, *Data Set of Channel Simulations of an Urban Platooning Scene at the 'Leipziger Platz' at the City Center of Berlin*, version 1.0.0, Zenodo, May 2021. [Online]. Available: <https://doi.org/10.5281/zenodo.4739568>.